

Numerical study on the effect of electrode force in small-scale resistance spot welding

B.H. Chang*, Y. Zhou

Department of Mechanical Engineering, University of Waterloo, Waterloo, Ont., Canada N2L 3G1

Abstract

Since electrode force is an important process parameter in small-scale resistance spot welding (SSRSW), its effects on the electrical, thermal and mechanical behavior of the welding process when using direct current have been studied numerically in the present paper using the finite element method. The variations of contact radius, current density distribution and temperature profile at the sheet/sheet (S/S) and electrode/sheet (E/S) interfaces, the threshold weld times and the maximum diameters of the weld nuggets under three different levels of electrode force are investigated. The calculated results show that increasing electrode force will increase the contact radius at the contact interfaces and decrease the welding current density, and hence delay nugget initiation and growth. Increasing electrode force also decreases the cooling rate at the nugget center after the welding current is turned off.

© 2003 Elsevier Science B.V. All rights reserved.

Keywords: Small-scale resistance spot welding; Electrode force; Finite element method; Contact radius; Current density; Temperature profiles

1. Introduction

Small-scale resistance spot welding (SSRSW) is one of the micro-joining processes, in which a weld is formed between two workpieces through the localized melting and coalescence of a small volume of the material(s) due to the resistance heating caused by the passage of an electric current [1,2]. SSRSW has been employed increasingly in the fabrication of electronic components and devices to join thin sheet metals of thickness less than 0.2–0.5 mm; however, despite the ever-increasing application, there is limited research work in this area. In comparison, extensive studies have been carried out on the “large-scale” resistance spot welding (LSRSW) of sheet metals thicker than 0.5 mm [3].

Recent studies on SSRSW have indicated that it is an unacceptable practice to “scale down” the welding procedures suggested for LSRSW in order to select process parameters for SSRSW since many differences existing between SSRSW and LSRSW [4–6]. Both experimental and numerical work has demonstrated the large difference in electrode force is the fundamental reason for the other differences between LSRSW and SSRSW [4–6] and the relatively small electrode force applied has a much larger influence

on the process in SSRSW. However, detailed studies are required to better understand the effects of electrode force in SSRSW.

It is well known that resistance spot welding (RSW) is a complex process in which coupled interactions exist between electrical, thermal, mechanical, and even metallurgical phenomena. Because of this complexity, it is very difficult to obtain insightful information of welding process through even the most ambitious experiments alone. On the other hand, numerical modeling provides a powerful tool in studying these interactions. In fact, this is the reason that, over the recent years, much development work has been carried out on the numerical modeling of LSRSW, in which more and more details in RSW have been taken into account in the computations [7–11]. However, little numerical work has been published for SSRSW in the open literature.

An incrementally coupled electrical–thermal–mechanical algorithm has been developed recently to simulate SSRSW using the finite element method [6]. The predicted nugget diameter in the SSRSW of mild steel using this finite element model compares well with experimental results. This numerical model is also employed to study the differences between SSRSW and LSRSW. The variations of contact radius, welding current density, and temperature profile at the sheet/sheet (S/S) interfaces are investigated and compared between these two processes. The computational results show that the difference in electrode force is the

* Corresponding author.

E-mail address: bhchang@mail.tsinghua.edu.cn (B.H. Chang).

essential reason for the other differences between LSRSW and SSRSW. Compared to LSRSW, the much lower electrode force applied in SSRSW results in a relatively small contact area and hence a much higher welding current density, which in turn leads to a faster heating rate and higher temperature at the S/S interface. A small contact area also results in a relatively small nugget size in SSRSW, which is only about 30–40% of the electrode tip diameter. In contrast, the nugget diameter in LSRSW is comparable to the electrode tip diameter. In this work, the previously developed finite element model will be used to further study the effects of electrode force in the SSRSW process.

2. Numerical modeling

2.1. Physical model

The set-up for SSRSW in this work is shown in Fig. 1. During the welding, an electrode force is applied to achieve good contact at the electrode/sheet (E/S) and S/S interfaces. Then, an electric current passes through top and bottom electrodes and heats the workpieces by Joule heating:

$$Q = I^2 R t \quad (1)$$

where Q is the heat generation, I the welding current, R the resistance, and t the duration of current (weld time). When the temperature at the S/S interface reaches the melting point of the material, a molten nugget begins to form and grow. When the welding current is turned off, this molten nugget will solidify to form a spot weld that joins the workpieces together. The electrode force is maintained during the whole process to ensure the electric current continuity,

and is continually applied for a short period after the current is turned off. Unlike LSRSW, no water is used to cool the electrodes because of the limited electrode dimensions in SSRSW.

Stepped electrodes (Class II) with a flat tip surface of 3.2 mm diameter and mild steel (AISI 1008) of 0.2 mm thickness are assumed in the computations. The temperature-dependent electrical, thermal and mechanical property parameters of the electrodes and workpieces are from Ref. [8]. Computations were conducted at three levels of electrode force (50, 100 and 150 N), with a direct current (DC) input of 1.0 kA.

2.2. Contact resistance model

As is well known, the resistance includes two bulk resistances of the electrodes, two bulk resistances of the workpieces, two contact resistances at the E/S interfaces and one contact resistance at the S/S interface. Both the electrodes and the sheet material have well-defined values of electrical resistivity together with other material properties. However, the contact resistances at the interfaces are not well defined. Several models have been developed to deal with the contact resistance [8–11], but almost all of the approaches involve a great deal of trial-and-error. To eliminate the uncertainty caused by the trial-and-error methods, a fundamental-based contact resistance model proposed by Li et al. [10] is used in the present computations (see Ref. [6] for details on how this contact resistance model is adopted in modeling SSRSW).

In this contact resistance model, the contact resistances are derived from the work of Kohlrausch [12], in which a relationship was developed between the voltage drop across a metallic contact interface and its resistance. According to the model, the voltage drop across the contact interface can be estimated by the following equation:

$$V^2 = 4L(T_S^2 - T_0^2) \quad (2)$$

where V is the voltage drop across the contact interface, and T_S and T_0 are the contact supertemperature and the bulk temperature at the interface, respectively. L is the Lorentz constant with a value of about $2.0 \times 10^{-8} (\text{V}/^\circ\text{C})^2$ for iron [13]. In the present computations, T_S at the S/S interface is specified to be the solidus of mild steel (1500°C), and that at E/S to be the melting point of the electrodes (1084°C).

From Eq. (2), one can obtain the voltage drop across the interface at any bulk temperature (T_0) below T_S . Based on this temperature-dependant voltage drop, the temperature-dependant contact resistance of the interface can be calculated by dividing by the welding current. Furthermore, the contact resistance value can be converted to an equivalent electrical resistivity using the geometrical information of the contact elements at the interfaces. For a temperature of above T_S , the contact resistance disappears, and the electric resistivity values of the mild steel sheets are used for the contact elements.

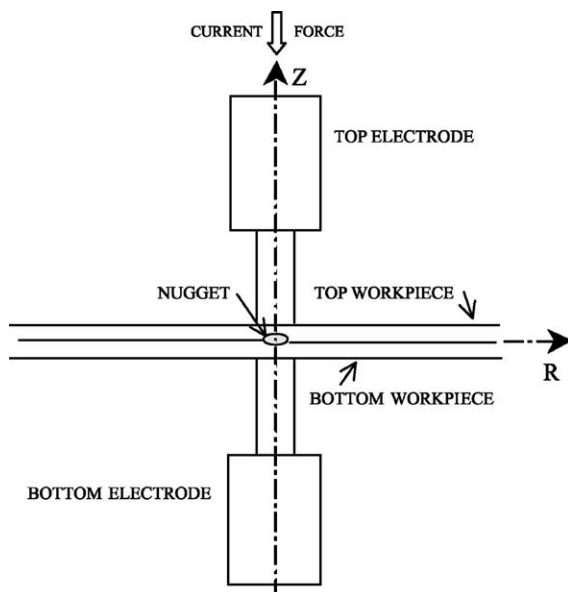


Fig. 1. Schematic set-up for RSWS.

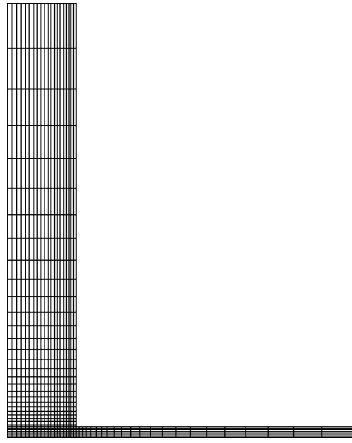


Fig. 2. Upper-half of the finite element mesh used in the computations.

2.3. Finite element model

In the numerical model, an initial mechanical status (contact area, stress and strain distribution, etc.) is first calculated. An electrical–thermal analysis is then used to calculate the Joule heating and temperature development at a small time increment. The temperature field calculated is then imposed into a thermal–mechanical analysis to calculate a new mechanical status that is updated in the electrical–thermal analysis to account for the variations of actual contact areas. This procedure continues until the welding process is completed.

Because of the axisymmetry of the welding set-up shown in Fig. 1, only one half of the model is considered. Fig. 2 shows the upper-half of the two-dimensional finite element meshes used in the computations. Three types of elements are used: a thermoelectric solid element for the thermal–electrical analysis; an isoparametric solid element for the thermal–mechanical analysis; and a node-to-surface contact element for coupling the two analyses. A layer of thermoelectric solid element of 0.01 mm thickness is used to simulate the contact resistance at the interfaces in the thermal–electrical analysis. The mesh structure consists of 1906 nodes and 1708 solid elements, which has been shown by a mesh convergence study to provide a sufficiently refined mesh. All computations were accomplished on a Pentium 500 personal computer.

In the electrical–thermal analysis, the electrical boundary conditions are set by a zero potential at the bottom end of the lower electrode, and a DC applied at the top end of the upper electrode. At the E/S and S/S interfaces, the current flow is only permitted across the areas where the E/S and S/S surfaces are in contact, while no current flow is allowed when those surfaces are separated. In the thermal–mechanical analysis, electrode force is applied as an evenly distributed pressure at the top end of the upper electrode. The axial displacements at the bottom end of lower electrode, together with the radial displacements of the central line, are all constrained.

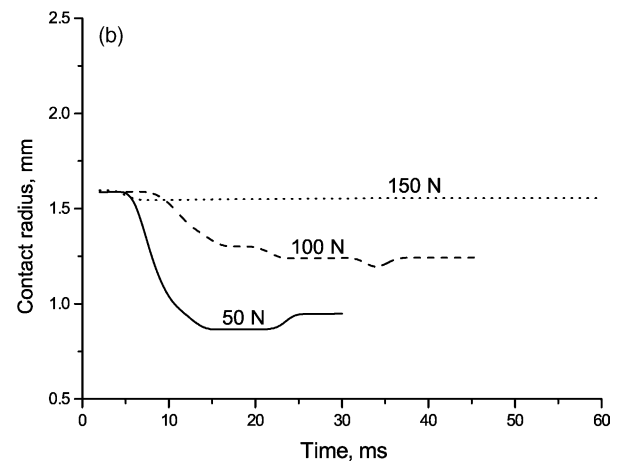
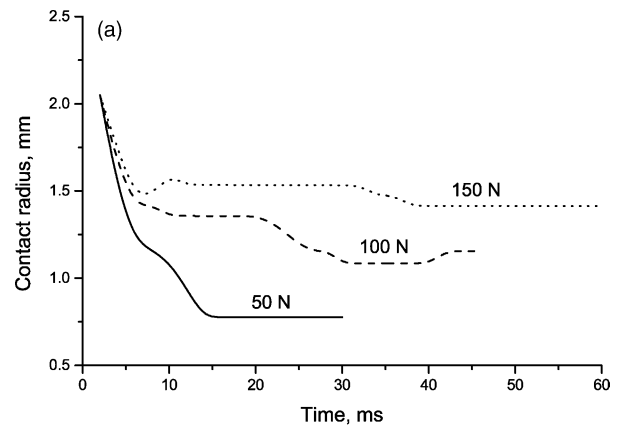


Fig. 3. Variations of contact radius at the: (a) S/S and (b) E/S interfaces under different electrode forces.

3. Results and discussion

3.1. Contact radius

Fig. 3 shows the variations of contact radius at both the S/S and E/S interfaces. For all three load levels, the initial contact radius at the S/S interfaces are larger than the electrode tip radius (Fig. 3(a)) because that the region outside the nominal contact radius (i.e., the electrode radius) is pushed into contact under the electrode force. The contact radius reduces greatly after a short period of heating, due to the uneven thermal expansion at the workpieces. The thermal heating at the central portion of the workpieces leads to a thermal expansion at the region and hence forces the two workpieces to become separated at the edge of the portion. It is obvious that the magnitude of the contact area depends on a balance between the electrode force applied and the force resulting from the uneven thermal expansion. The contact radius continually decreases but at a relatively slower rate until it reaches a minimum value (Fig. 3(a)), after which the contact radius increases slightly due to the softening of the workpieces at high temperature.

While the variations of contact radius demonstrate the similar trend for different electrode forces, a large difference exists in the minimum contact radius when the electrode forces are different. The reduction in contact radius is the most significant when the electrode force is 50 N with a minimum contact radius of about 50% of the electrode tip radius. Increasing the electrode force increases the minimum contact radius. As can be seen, the minimum contact radius is about 90% of the electrode radius when increasing the electrode force to 150 N. This is already similar to the LSRSW situation, where the minimum contact radius is almost equal to the electrode radius at the S/S interface [6].

The variations of contact radius at the E/S interface under three different levels of the electrode forces are shown in Fig. 3(b). For all three cases, it can be found that the contact radius is equal to the electrode tip radius at the beginning of welding at different electrode forces. When the welding current is applied, the contact radius begins to decrease due to the thermal expansion of the workpieces, which is similar to what happens at the S/S interface. However, the decrease in contact radius is different for different electrode forces. The decrease with lower electrode force (50 N) is much more significant than that with higher electrode force (150 N). When the electrode force is 150 N, it is again very similar to LSRSW where there is a little change in contact area at the E/S interface [6]. Comparing Fig. 3(a) and (b) indicates that, under the same electrode force, the contact radius at the E/S interface is larger than that at S/S interface, except at the beginning of welding when the contact radius at the S/S is larger.

3.2. Welding current density

Fig. 4 shows the changes in the distribution of welding current density at different weld times when the electrode force is 50 N. The nominal current density, which is defined by the welding current divided by the cross-section area of the electrodes, is about 124 A/mm².

At the beginning of welding, the current density distributes evenly at the S/S interface and is below the nominal value (124 A/mm²) due to the larger contact area than the electrode tip surface (Fig. 3(a)). The current density then increases rapidly due to the reduction in the contact area. For example, the current density when the weld time is 10 ms is almost double the nominal current density because of the actual contact area (with a radius of 1.1 mm) is about one-half of the electrode tip surface (Fig. 4(a)). The current density is also higher towards the central portion of the contact area because the temperature is higher in the portion and hence the contact resistance is lower. Once a molten nugget is formed, the current density concentrates in the nugget region because the contact resistance disappears in the region (e.g., when the weld time is 20 ms in Fig. 4(a)). It is also interesting to note that a current peak exists at the periphery of the nugget because the current tends to flow into this low resistance region [6]. Therefore, the current density distribution

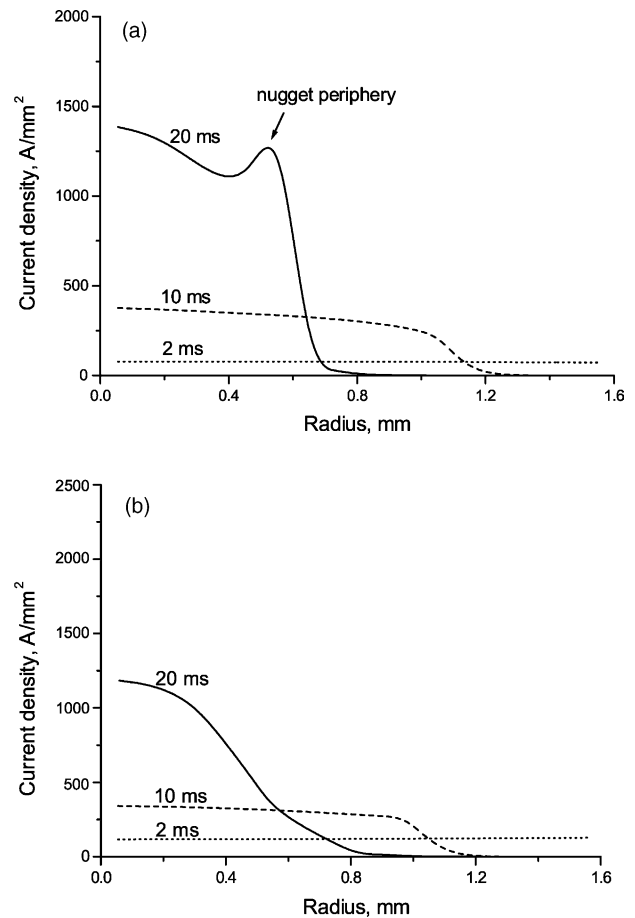


Fig. 4. Variations of current density distribution at the: (a) S/S and (b) E/S interfaces at different welding times with electrode force of 50 N.

is affected by both contact area and temperature-dependent resistances (both contact and bulk). Similar trends in the changes of the current density distribution have been observed at the E/S interface except for no melting occurs at the interface (Fig. 4(b)).

When the electrode force is varied, the evolution pattern of the current density distribution stays unchanged; however, the time scales of the pattern are different (Fig. 5(a)). For example, when the weld time is 25 ms, a current density concentration (larger than 1000 A/mm²) occurs at the S/S interface when the electrode force is 50 or 100 N while the current density is still distributed evenly when the electrode force is 150 N. At the E/S interfaces, the current density is also higher when the electrode force is lower because of the smaller contact area (Fig. 5(b)).

3.3. Temperature distribution and nugget formation

The thermal history in RSW determines a number of metallurgical behaviors of the joint (e.g., the diameter of the molten nugget, and weld and heat-affected zone microstructure) and hence affects the joint quality. Fig. 6 shows the development of the temperature profiles at the S/S and E/S

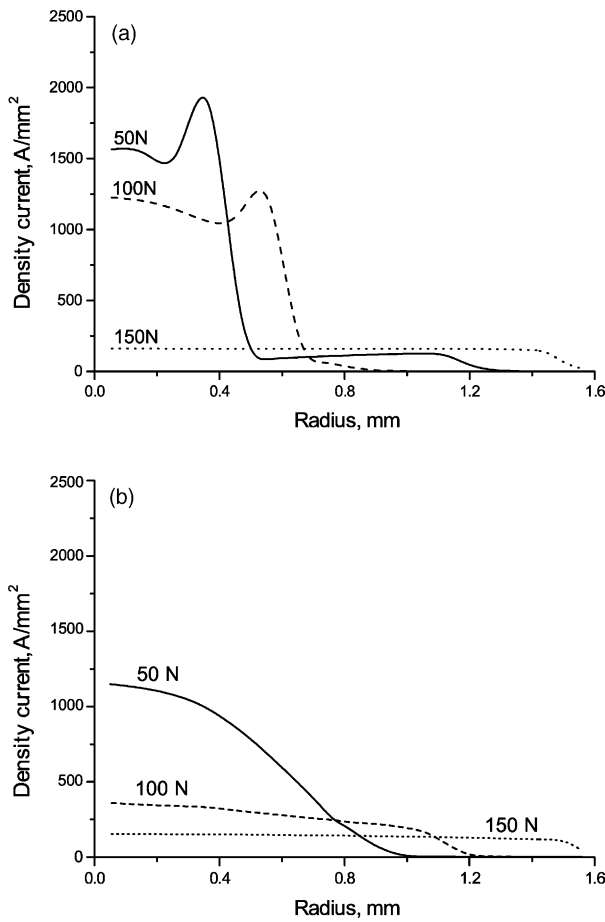


Fig. 5. Distributions of welding current density at: (a) S/S and (b) E/S interfaces under different electrode forces for weld time of 25 ms.

interfaces when the electrode force is 50 N. At the S/S interface, the workpieces are heated evenly at the beginning of welding (e.g., when the weld time is 2 ms in Fig. 6(a)). As the weld time increases, the temperature at the center of the workpieces increases more rapidly than that at the edge due to two reasons. First, the heat loss is more significant at the edge resulting from the heat transfer to the outside portion of the workpieces. Second, the current density is higher at the center and hence the central part is heated more intensively. Once the hottest point (i.e., at the center of the workpieces in Fig. 6(a)) reaches the melting point of the workpieces and a molten nugget is formed. This nugget grows very rapidly initially and reaches its maximum diameter within a very short period (e.g., only about 3 ms in Fig. 6(a)). The nugget grows little after 14 ms, which indicates that the system has almost reached a thermal equilibrium.

Similar to that at the S/S interface, a uniformly distributed temperature at the E/S interface can be seen at the beginning (Fig. 6(b)), and then the temperature increases more quickly at the center than that at the edge. Obviously, the temperature at the E/S interface is much lower than that at the S/S surface due to the much better thermal conductivity of the electrodes. The variations of the temperature profiles at the E/S and

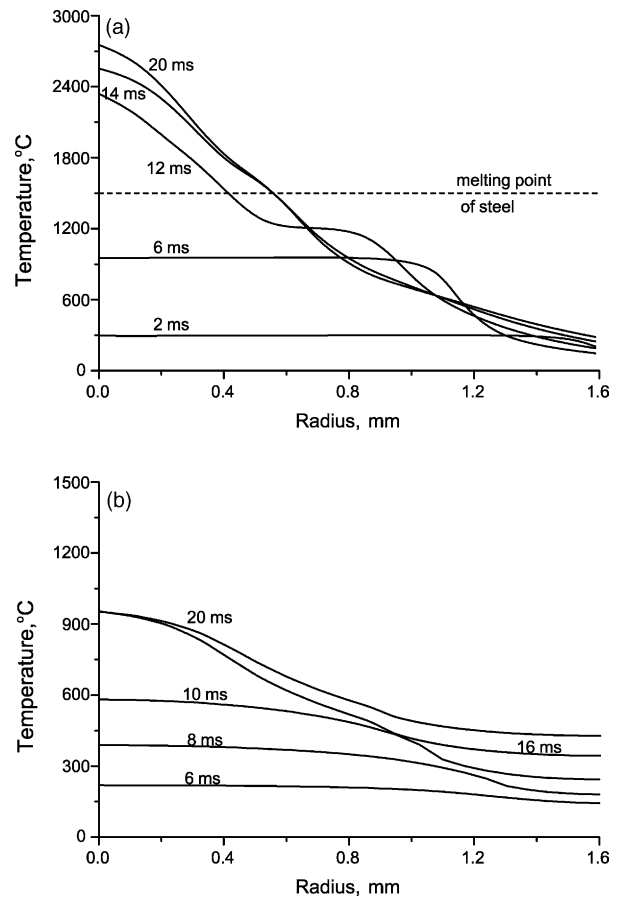


Fig. 6. Temperature distributions at: (a) S/S and (b) E/S interfaces at different welding time when the electrode force is 50 N.

S/S interfaces at different electrode forces have basically observed the same pattern as those in Fig. 6.

Fig. 7 shows the thermal cycles of the central points at the S/S and E/S interfaces under different electrode forces. The computations also include the cooling period in which that welding current is turned off while the electrode force is still applied. At the S/S interface (Fig. 7(a)), decreasing electrode force increases the heating rate and decreases the time required for nugget initiation (from 10 ms when the electrode force is 50 N to 42 ms when the electrode force is 150 N). This is obviously due to the smaller contact area (Fig. 3) and hence the higher current density (Fig. 5) when the electrode force is decreased. If the weld time is kept constant, it can be deduced that the threshold welding current will increase when the electrode force is decreased since the heat generation is proportional to the welding current and weld time, as shown in Eq. (1).

In practice, a shorter threshold weld time indicates a faster production rate, and a lower threshold welding current indicates that a welding machine with a smaller capacity could be used if the electrode force is decreased. However, too low an electrode force may result in other problems, such as an increased electrode–sheet sticking [4,5]. The peak temperature at the nugget centers is also higher when the electrode

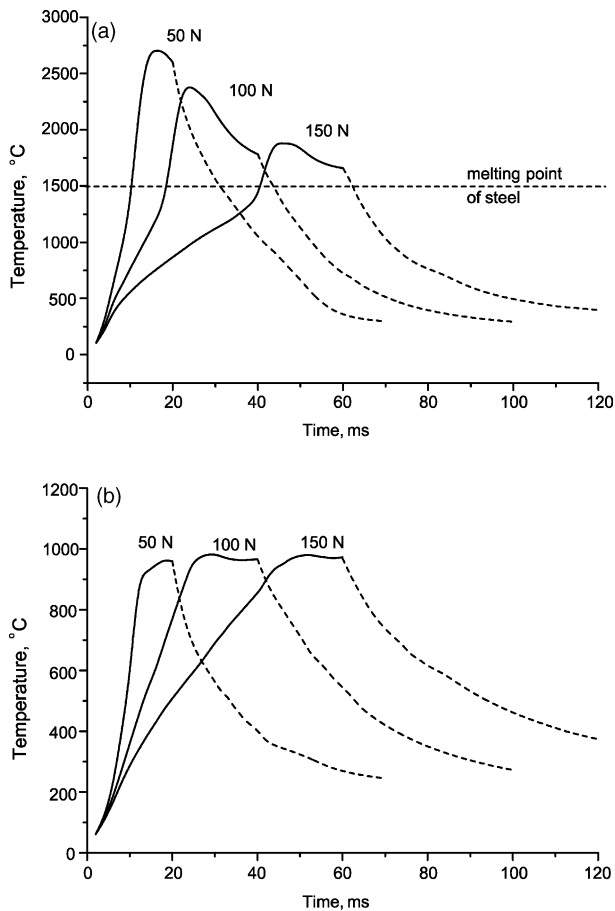


Fig. 7. Temperature history of the central point at: (a) S/S and (b) E/S interfaces (dashed lines indicate the welding current is off).

force is lower (Fig. 7(a)). The temperature at the nugget centers starts to decrease even before the welding current is turned off. This is resulted from the decreased heat generation because of the increased nugget diameter and the relatively even distributed current density. Increasing electrode force also decreases the cooling rate at the nugget center, which may be beneficial when welding a material that will experience solid-state phase transformation(s) during the cooling period [3]. However, the effect of electrode force on the cooling rate in this study is very small when welding high-strength low-alloy steels because all three cooling rates are much faster than the critical rate to form brittle microstructure [3]. Other methods (such as long weld time) are required to slow down the cooling rate when welding high-strength low-alloy steels [3]. Similar to the S/S interface, the heating rate at the central point at the E/S interface is also decreased with an increasing electrode force (Fig. 7(b)), which can be also attributed to the increased contact area and hence decreased current density when the electrode forces is increased. However, the electrode force has little effect on the peak temperature at the E/S interfaces (Fig. 7(b)).

Fig. 8 shows the nugget initiation and growth when the electrode force is varied. It can be seen that after the melting

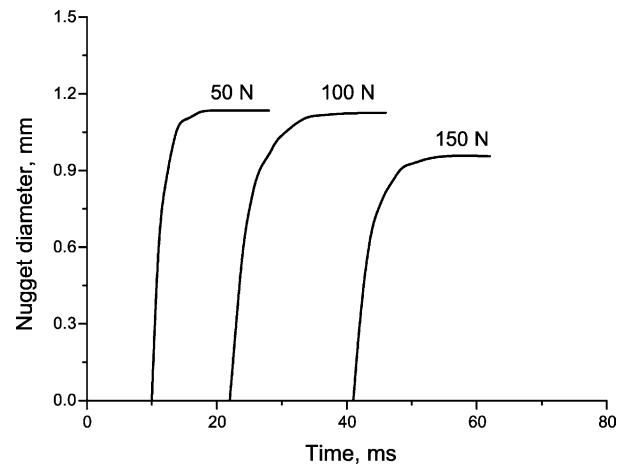


Fig. 8. Nugget initiation and growth under different electrode forces.

begins at different threshold weld times, the nugget grows very rapidly and reaches its maximum diameter within a very short period. Further increasing the welding time will not increase the nugget diameter and contribute to the joint strength because the nugget size and the joint strength is correlated [14]. The maximum nugget diameter formed under 150 N is a little smaller than that formed under 50 N because of the larger contact area and lower current density under higher electrode force; however, the effect is relatively small.

4. Concluding remarks

The effects of electrode force on the SSRSW process when using a DC is investigated using the finite element method. The variations of contact radius, current density distribution and temperature profile at the S/S and E/S interfaces, the threshold weld times and the maximum diameters of the weld nuggets under different electrode forces are investigated. The main results are summarized as follows:

1. The contact radius at both E/S and S/S interfaces decreases during the welding process. Increasing electrode force increases the contact radius at both interfaces. The minimum contact radius at the E/S interface is larger than that at the S/S interface.
2. The welding current density distributes evenly initially, and then increases with the decreasing of contact area at both interfaces and finally concentrates at the molten nugget region. Increasing electrode force decreases the current density because of the increased contact area.
3. The temperature at the central part of the workpieces is the highest at both interfaces. A molten nugget initiates at the S/S interface center. The temperature increase more quickly under a lower electrode force because of the decreased contact area and increased current density.
4. A shorter threshold weld time or lower threshold welding current is needed for nugget initiation when the electrode

force is decreased. However, decreasing electrode force also increases the cooling rate at the nugget center.

Acknowledgements

The authors would like to acknowledge the financial support from the Natural Sciences and Engineering Research Council (NSERC), Canada.

References

- [1] K.I. Johnson (Ed.), *Introduction to Microjoining*, TWI, 1985.
- [2] C.A. Harper, *Handbook of Materials and Processes for Electronics*, McGraw-Hill, New York, 1970.
- [3] RWMA, *Resistance Welding Manual*, 4th ed., Resistance Welder Manufactures Association, Philadelphia, PA, 1989, Chapter 14.
- [4] Y. Zhou, P. Gorman, W. Tan, K.J. Ely, *J. Electron. Mater.* 29 (9) (2000) 1090–1099.
- [5] K.J. Ely, Y. Zhou, *Sci. Technol. Weld. Join.* 6 (2) (2001) 63–72.
- [6] B.H. Chang, M.V. Li, Y. Zhou, *Sci. Technol. Weld. Join.* 6 (5) (2001) 1–8.
- [7] H.A. Nied, *Weld. J.* 63 (4) (1984) 123-s–132-s.
- [8] C.L. Tsai, O.A. Jammal, J.C. Papritan, D.W. Dickinson, *Weld. J.* 71 (2) (1992) 47-s–54-s.
- [9] D.J. Browne, H.W. Chandler, J.T. Evans, J. Wen, *Weld. J.* 74 (10) (1995) 339s–344s.
- [10] M.V. Li, P. Dong, M. Kimchi, in: *High-Productivity Joining Processes*, Proceedings of the ICAWT'97, Columbus, OH, September 17–19, 1997, pp. 357–369.
- [11] Z. Feng, J.E. Gould, S.S. Babu, M.L. Santella, B.W. Riemer, in: *Proceedings of the Conference on Trends in Welding Research*, Pine Mountain, GA, 1998, American Society of Metals, Cleveland, OH, pp. 599–604.
- [12] F. Kohlrausch, *Über das problem eines elektrisch erwarmten leiters*, *Ann. Phys. Lpz.* 1 (1900) 312.
- [13] H.N. Wagar, in: D. Baker, et al. (Eds.), *Integrated Device and Connection Technology*, Prentice-Hall, Englewood Cliffs, NJ, 1971, pp. 439–499.
- [14] *Welding Process*, vol. 2, 8th ed., AWS, *Welding Handbook*, American Welding Society, Miami, 1991.